



Student Symposium

Wednesday, June 22

Session I

SL1

MICROSTRUCTURE OF THIN LAYERS OF GOLD AND GOLD NANOPARTICLES

T. Košutová¹, Z. Krťouš¹, J. Kousal¹, O. Kylián¹, J. Hanuš¹, L. Martínez², Y. Huttel²,
D. Nikitin¹, H. Biederman¹, P. Pleskunov¹, L. Horák¹, M. Dopita¹

¹Charles University in Prague, Faculty of Mathematica and Physics, Czech Republic

²Instituto de Cienciade Materialesde Madrid (ICMM-CSIC), Madrid, Spain

In the presented study, we investigated differences in the microstructure of thin gold layers and layers of gold nanoparticles with a focus on their thermal development. Thin films composed of nanoparticles are interesting for applications because of their inherent high porosity, which is essential for gas sensing, efficient batteries, catalysis or hydrogen storage applications. The thermal stability of nanoparticle layers depends on chemical and phase composition, the configuration of nanoparticles or the atmosphere in which they are heated up and it is critical for multiple applications of gold nanoparticles.

The homogeneous gold nanoparticles in our study were prepared by magnetron sputtering from pure metal targets followed by aggregation of fragments to the metallic clusters, by so-called gas aggregation cluster sources. The gold thin films for comparison were prepared by evaporation and by sputtering. A Series of samples with various thicknesses deposited on silicon substrates were characterized

after preparation and also under annealing up to 1000 °C in the air atmosphere.

Size distribution and morphology of nanoparticles were determined by small angle X-ray scattering (SAXS), atomic force microscopy (AFM) and confirmed by scanning electron microscopy measurements (SEM) for ex-situ annealed samples. In-situ measurements of X-ray diffraction were used to characterize the thermal evolution of lattice parameters, microstructural defects and sizes of crystallites.

The as-deposited gold nanoparticles contain a large amount of stacking faults (up to 6 %) and also significant microstrain in the crystal structure. During annealing, ordering of the structure is observed together with the step-like increase of the sizes of crystallites following the increase of the sizes of whole nanoparticles. The occurrence of the holes in the substrates after heating to the highest temperatures was successfully explained.

SL2

STRUCTURAL DEFECTS IN SiC AND Ge MICROCRYSTALS

M. Podhorský, M. Meduňa

Department of Condensed Matter Physics, Masaryk University, Brno, Czech Republic
martinpodhorskyj@gmail.com

Reciprocal space mapping (RSM) is a method of X-ray analysis which can provide us with useful structural information about studied samples, such as mismatch, strain, relaxation and defects of epitaxial grown layers on a substrate [1].

The studied samples consisted of large array of Ge and SiC microcrystals grown by Low-energy plasma-enhanced chemical vapor deposition (LEPECVD) technique [2]. This method enables fast, low-temperature epitaxial growth of crystals onto micrometer-scale tall pillars etched into Si(001). The method was developed at ETH Zürich, where the samples were also prepared in the group from H. von Känel [3]. It enables to grow relatively thick layers with different lattice parameters of high structural quality [3, 4]. The samples were subjected to X-ray study in order to obtain structural information.

In our experiment we used Rigaku SmartLab diffractometer, which uses X-ray source with characteristic wavelength of 0.154 nm and a hybrid multi-dimensional pixel detector HyPix-3000. The data acquisition by the detector can be done in 0D, 1D and 2D regime. For our analysis we opted for the linear regime. We placed the sample on a goniometric table and put a series of linear slits and monochromators between the source, sample and the detector. First we measured QxQz reciprocal space maps (RSMs) around symmetric and asymmetric diffractions of the samples at two different azimuths (0 and 90 particularly and (224) for Ge and (004) and (113) for SiC, from which we obtained the lattice parameter, strain and relaxation of the array of microcrystals.

The next part of our measurement was aimed to obtain RSMs of the samples in the plane parallel to sample surface

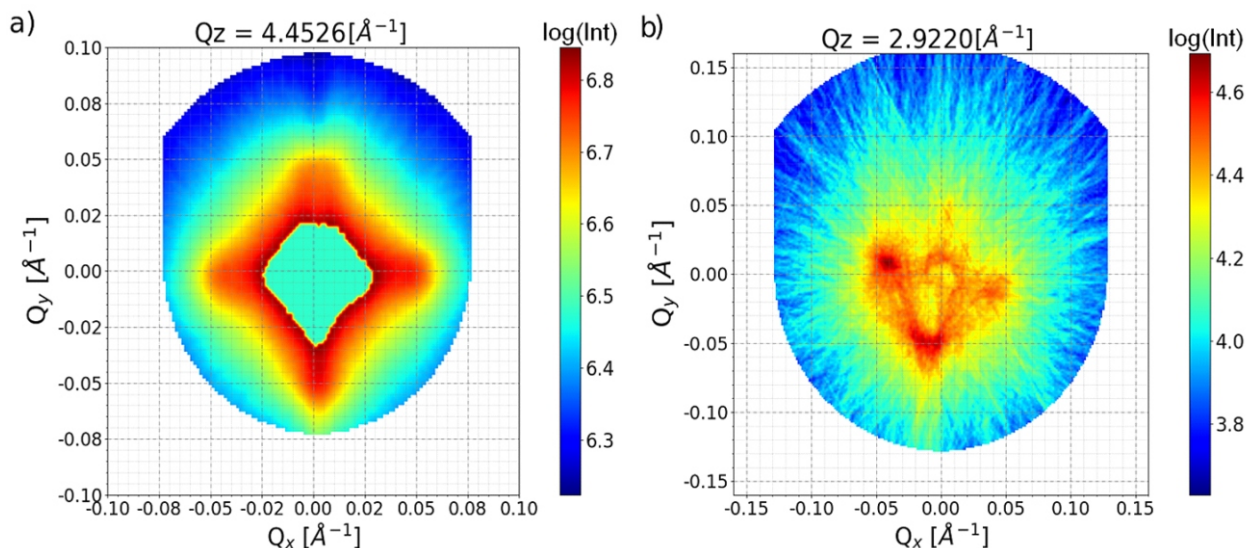


Figure 1. Q_xQ_y RSMs for a) Ge and b) SiC samples. In a) the maximum was cut out in order to showcase the satellite maxima. The maxima originate from crystal lattice bending and they copy a four-fold symmetry of microcrystal geometry. The satellite maxima in b) correspond to cuts through streaks $\{111\}$ originating from defects (stacking faults) in the SiC microcrystal layer [7].

(Q_xQ_y). This is impossible to do with standard laboratory set-up, which enables us to measure only the Q_xQ_z plane of the reciprocal space. One way of obtaining the Q_xQ_y RSM for certain Q_z is to measure multiple Q_xQ_z RSMs at different azimuthal rotations and transforming them using Radon transform [5]. Radon transform is a mathematical method used to construct 3D intensity images from 2D slices, commonly used in computer tomography [6].

We measured RSM of one diffraction maximum, particularly (004) and (002) for Ge and SiC respectively, at different azimuths ranging from 0 up to 180 with a 2 step. The Q_xQ_z RSMs measured at different azimuthal angles were transformed into a series of sinograms, from which it was possible to obtain series of Q_xQ_y RSMs for the measured range of Q_z positions. Examples of reconstructed Q_xQ_y RSMs are shown in Figure 1.

The obtained Q_xQ_y RSMs for different Q_z form set of slices through the reciprocal space which can generally build a 3D RSM. The distribution of scattered intensity in 3D reciprocal space can then provide another view on analysis of structural defects such as local lattice strain, misfit dislocations or stacking faults present in the studied samples.

1. U. Pietsch, V. Holý, T. Baumbach, *High-Resolution X-Ray Scattering*, Springer New York, NY, 2004.
2. C. Rosenblad, H.R. Deller, T. Graf, E. Müller, H. von Känel, *Journal of Crystal Growth* **188**, (1998), 125.
3. C.V. Falub, H. von Känel, F. Isa, R. Bergamaschini, A. Marzegalli, D. Chrastina, G. Isella, E. Müller, P. Niedermann, L. Miglio, *Science*, **335**, (2012), 1330.
4. H. von Känel, L. Miglio, D. Crippa, T. Kreiliger, M. Mauceri, M. Puglisi, F. Mancarella, R. Anzalone, N. Piluso, F. La Via, *Materials Science Forum* **821–823**, (2015), 193.
5. M. Meduña, F. Isa, F. Brennan, H. von Känel, *J. Appl. Cryst.* **55**, (2022) in print.
6. P. Suetens, *Fundamentals of Medical Imaging*, Cambridge University Press, 2009.
7. M. Meduña, T. Kreiliger, M. Mauceri, M. Puglisi, F. Mancarella, F. La Via, D. Crippa, L. Miglio, H. von Känel, *Journal of Crystal Growth* **507**, (2019), 70.

We acknowledge Claudiu V. Falub and Hans von Känel for providing the SiC and SiGe microcrystal samples.



SL3

SIZE DEPENDENCE OF SURFACE SPIN DISORDER IN FERRITE NANOPARTICLES

M. Gerina¹, M. S. Angotzi², V. Gajdošová³, M. Dopita⁴, D. Zákutná^{1*}

¹Faculty of Science, Charles University, Prague, Czech Republic

²Faculty of Chemical and Geological Science, University of Cagliari, Monserrato, Italy

³Polymer Morphology, Institute of Macromolecular Chemistry CAS, Prague, Czech Republic

⁴Faculty of Mathematics and Physics, Charles University, Prague, Czech Republic

Surface spin disorder or canting arises from the breaking of exchange bonds and the breaking symmetry of the lattice, and thus crucially determines the performance of magnetic nanoparticles (NPs) and their potential technological and biomedical applications [1, 2]. Despite an enormous interest and technological relevance of magnetic NPs, there is still a lack of knowledge on the magnetic NPs spin structure. Due to the surface-to-volume ratio, surface effects will be closely related to the particle and coherent domain size. However, it is difficult to isolate the surface contribution from the bulk effects using macroscopic magnetization techniques, such as magnetization measurements, ferromagnetic resonance, Mössbauer spectroscopy [3], X-ray magnetic circular dichroism [4], and electron energy loss spectroscopy [5]. A spatially resolved magnetization is required to unveil and disentangle the surface contribution. Half-polarized small angle-neutron scattering (SANSPOLE) enables us to investigate the magnetization on the nanometer scale [6]. Our previous study has proven that the magnetic volume in ferrite NPs is not fixed at the coherent domain size but increases with the applied magnetic field [7]. This implies that the applied magnetic fields polarize the disordered surface spins, leading to an increase in the magnetic size of the NPs [7].

In this contribution, we will present the size dependence of the disorder energy and the surface anisotropy in spherical CoFe_2O_4 NPs with different coherent domain sizes range of 3.1(1), 6.3(2), and 8.6(1) nm synthesized using the oleate-based solvothermal method [8] with narrow size distribution confirmed by transmission electron microscopy (TEM) and small-angle X-ray scattering (SAXS). Rietveld's analysis shows that coherent domain size is

smaller than mean particle size, suggesting a possible presence of a spin disorder or canting. The spatial magnetization distribution obtained from SANSPOLE reveals significant magnetic field dependence of magnetized volume for each sample, but with different degrees of the total magnetized NP volume. Ultimately, we will discuss the particle and coherent size dependence of the surface anisotropy constant.

We greatly acknowledge Dr. Jana Havlíčková for the TGA analysis, and Dušan Rohal' for synthesizing 1 samples. We acknowledge the Institut Laue-Langevin, Grenoble, France for the provision of beamtime at the instrument D33 and Dr. Nina J. Steinke for the technical support at the instrument.

1. E. Tronc et al., Journal of Magnetism and Magnetic Materials **221** (2000) 6379.
2. A. Omelyanchik et al., Nanomaterials. **10** (2020) 1288.
3. B. N. Pianciola et al., J. Magn. Magn.Mater. **377** (2015) 44.
4. V. Bonanni et al., Appl. Phys. Lett. **112** (2018) 022404.
5. D. S. Negi et al., Phys. Rev. B **95** (2017) 174444.
6. S. Mühlbauer et al., Rev Mod Phys. **91** (2019) 015004..7. D. Zákutná et al., Phys Rev X. **10** (2020) 031019.
8. M. Sanna Angotzi et al., J. Nanosci. Nanotechnol. **19** (2019) 4954.

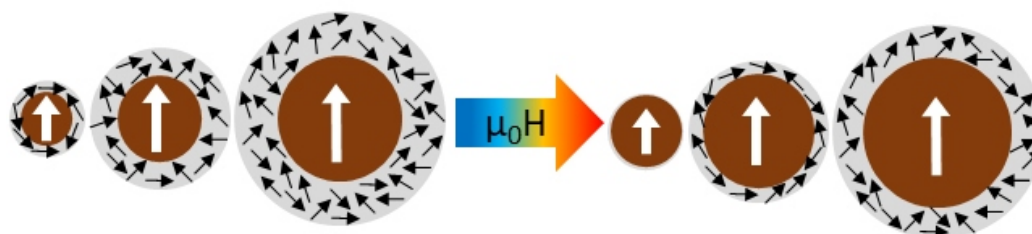


Figure 1. Schematic presentation of the size dependence of magnetized volume growth in applied magnetic field. Grey and brown particle part corresponds to the disorder and magnetized volume of nanoparticles.

SL4

METAL CARBOXYLATES IN PAINTINGS – THE STUDY OF THEIR STRUCTURE AND BEHAVIOUR

Ruslan Barannikov^{1,2}, Petr Bezdička¹, Eva Kočí¹, Silvia Garrappa¹, Libor Kobera³,
Jan Rohlíček⁴, Jiří Plocek¹, Silvie Švarcová¹

¹*Institute of Inorganic Chemistry of the Czech Academy of Sciences, ALMA Laboratory, Husinec-Řež 1001, 250 68 Husinec-Řež, Czech Republic*

²*Department of Inorganic Chemistry, Faculty of Science, Charles University in Prague, Hlavova 2030/8, 128 43 Prague 2, Czech Republic*

³*Institute of Macromolecular Chemistry of the Czech Academy of Sciences, Heyrovského nám. 2, 162 06 Praha 6, Czech Republic*

⁴*Institute of Physics of the Czech Academy of Sciences, Na Slovance 1999/2, 182 21 Praha 8, Czech Republic*
barannikov@iic.cas.cz

Saponification, resulting from pigment-binder interactions is one of the most dangerous degradation phenomena affecting the appearance and stability of paintings. The crystallization of metal carboxylates (soaps) is assumed as a critical point for the development of undesirable changes manifested as protrusions, efflorescence, darkening and etc. However, factors triggering this process are not fully understood, limiting the development of a suitable strategy for conservation and preservation of precious works of art.

Previous research of the portrait miniatures [1] has revealed presence of different types of crystalline metal carboxylates frequently in a conjoined occurrence of lead white ($2\text{PbCO}_3 \cdot \text{Pb}(\text{OH})_2$) and cinnabar (HgS) pigments in paint layers, exceptionally even without presence of any lead-based pigment. These findings indicated that HgS assists to the formation of Pb and/or Hg carboxylates. Nevertheless, its role in the reaction mechanism has to be clarified.

The paucity of reliable reference structural data limited the experimental research of HgS effect on the pigment-binder interactions on molecular level. In our previous research [2], the long chain simple and mixed mercury (II) carboxylates in the series $\text{Hg}(\text{C16})_x(\text{C18})_{2-x}$ ($x=0.0;$

$0.2; 0.5; 0.8; 1.0; 1.2; 1.5; 1.8; 2.0$) were synthesized in the form of pure polycrystalline powders and characterized by XRPD, ssNMR, FTIR and DSC. The crystal structure of the studied mercury carboxylates was described on the basis of complementary ssNMR and XRPD measurements, Rietveld refinement and DFT calculations. All the subjected compounds crystallize in a monoclinic lattice of the $C2/c$ symmetry. Mercury atoms are arranged in a slightly distorted square antiprismatic geometry and are monodentatically bonded to carboxylate anions. The structural disorder at the aliphatic end of the stearic acid chains was detected in the mixed carboxylates.

The synthesized and characterized metal carboxylates were applied for the study of formation of metal soaps in model experiments simulating egg and/or oil-based paint systems consisted of lead and/or mercury-based pigments, and furthermore for the study of their crystallization in oil-based polymeric matrix.

1. S. Garrappa, D. Hradil, J. Hradilová, et al., *Anal. Bioanal. Chem.*, 2021, 413, 263-278.
2. R. Barannikov, E. Kočí, P. Bezdička, et. al. *Dalton Trans.*, 2022, 51, 4019–4032.



SL5

TEMPORAL EVOLUTION OF OPTICAL ABSORPTION AND EMISSION SPECTRA OF THIOL CAPPED CdTe QUANTUM DOTS

S. Gupta¹, S. Tomar^{2,3}, A. Priyam⁴, B. Bhushan⁵, A. Singh⁶, U. K. Dwivedi⁷, R. K. Choubey²

¹Department of Condensed Matter Physics, Faculty of Mathematics and Physics, Charles University, Ke Karlovu 5, Prague- 12116, Czech Republic

²Department of Physics, Amity Institute of Applied Sciences, Amity University, Noida Sector 125, Uttar Pradesh- 201313, India

³Applied Science and Humanities Department, ABES Engineering College, Campus- 1, 19thKM stone NH-24, Ghaziabad, Uttar Pradesh- 201009, India

⁴Department of Chemistry, School of Physical and Chemical Sciences, Central University of South Bihar, SH- 7, Gaya-Panchapur Road, Gaya, Bihar- 824236, India

⁵Department of Physics, School of Applied Sciences, Kalinga Institute of Industrial Technology, Bhubaneswar, Odisha- 751024, India

⁶Department of Physics, Faculty of Natural Sciences, Jamia Millia Islamia, Central University, New Delhi- 110025, India

⁷Department of Applied Physics, Amity School of Applied Sciences, Amity University Jaipur, Rajasthan- 303002, India
suhaas96@gmail.com

Quantum dots (QDs) are strongly confined semiconductor nanoparticles that exhibit novel and size-tunable properties as a result of quantum confinement effects in the particle size regime comparable to their Bohr excitonic radius. QDs have been rigorously studied to employ their desirable properties in optoelectronic devices; these very same size-tunable optoelectronic properties have also been investigated for potentially widespread use in sensing and imaging applications in biological systems [1-3]. CdTe is such a II-VI semiconductor compound, whose particle size can be tailored to exhibit luminescence across the visible spectrum [4]. However, to make CdTe a suitable material to be used in biological systems, it must be made water-soluble with the use of a biocompatible ‘capping’ material; capping the CdTe QD also affords it increased mechanical, chemical and luminescent stability [5]. The choice of functional group of the material used to cap the CdTe QD also lends to it easily tuneable surface properties that can be

used in biomedical tracking and drug delivery applications [6].

In the present work, we have synthesised and studied a series of CdTe QDs capped with four different thiols: (i) Thioglycolic acid (TGA), (ii) Mercaptoethyl amine (MEA), (iii) L-Cysteine (L-Cys), and (iv) Glutathione (GSH). An aqueous route was employed to synthesise all the samples, with varying reflux times for the different thiols used for capping. Fig.1 illustrates the confirmation of the cubic CdTe phase of the seed material from the XRD analysis of the synthesised CdTe@TGA QDs refluxed for 15mins; highest intensity characteristic (111) peak was further analysed to calculate the lower limit of crystallite size (2.4nm), interplanar spacing (3.65 Å), lattice constant (6.32 Å), microstrain and dislocation density. HRTEM and SAED studies further supported the results obtained from the XRD analysis. Fig.2 shows the comparison of the FTIR spectra of the CdTe@MEA QDs with the FTIR spectra of MEA; evidence of cleavage of the H-SR bond in thiols and simultaneous formation of the Cd-SR bond was used to

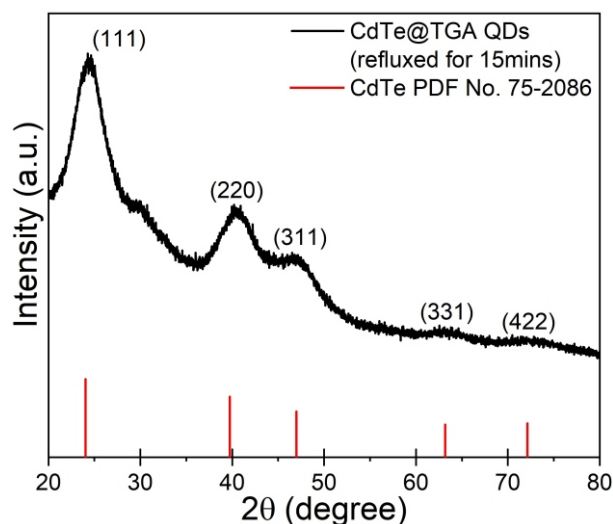


Figure 1. XRD analysis of the synthesised CdTe@TGA QDs refluxed for 15mins

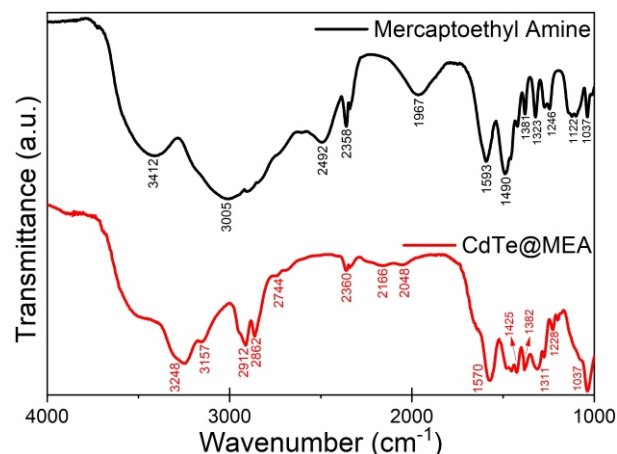


Figure 2. Comparison of the FTIR spectra of the synthesised CdTe@MEA QDs with the FTIR spectra of MEA

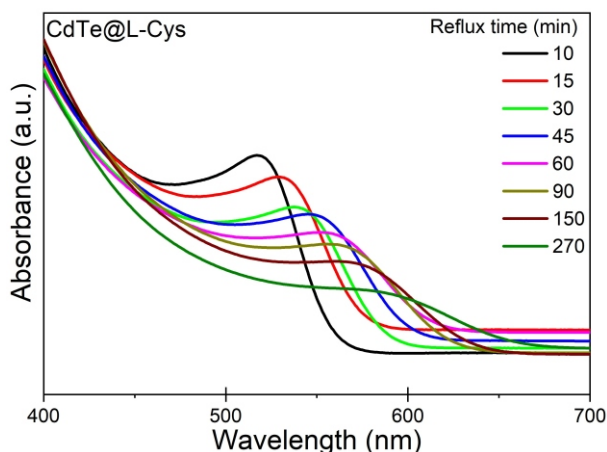


Figure 3. UV-visible absorption spectra of the synthesised CdTe@L-Cys QDs refluxed for different times.

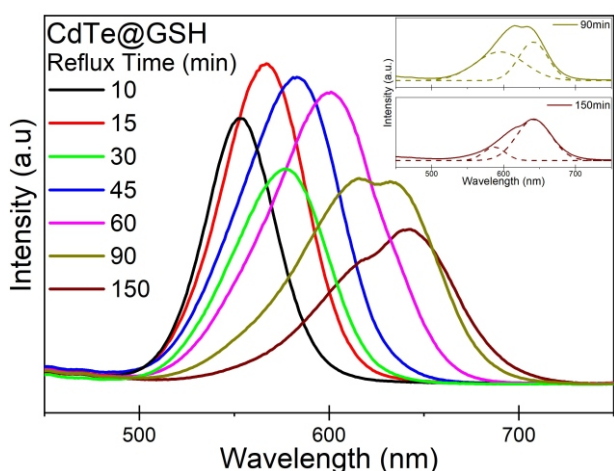


Figure 4. Photoluminescent emission spectra of the synthesised CdTe@GSH QDs refluxed for different times. Inset shows the deconvolution of the emission peaks at longer reflux times.

confirm the successful capping of all the thiols to the surface of the CdTe QDs.

Fig.3 shows the UV-visible absorption spectra of the synthesised CdTe@L-Cys QDs refluxed for different times. All synthesised samples exhibited blue-shift in absorption edge as compared to the bulk CdTe, confirming the strong size confinement of the nanoparticles; with increasing reflux time, the absorption edge shifted gradually to longer wavelengths for all samples. Band-gap energy was obtained from the Gaussian-fitted peak position of the 1st derivative of absorption v/s energy plot; tight binding

approximation model was used to calculate the size of the QD from the band gap energy. Particle size growth with increasing reflux time was observed for all samples: CdTe@GSH reached a predetermined particle size (4nm) the fastest (90mins) when compared to the other thiol capped CdTe QDs, while the CdTe@MEA QDs were unable to attain the same particle size even after 390mins of reflux time. To understand the growth mechanics, variations of concentration and particle size distribution of the synthesised thiol-capped CdTe QDs with respect to increasing reflux time and particle size was studied. Evidence of separation between the nucleation and growth processes, and identification of three distinct growth regimes (focusing, defocusing and equilibrium) allowed us to confirm the dominance of Ostwald ripening processes during the particle growth.

Fig.4 shows the photoluminescent emission spectra of the synthesised CdTe@GSH QDs refluxed for different times. At shorter reflux times, all samples exhibit narrow-width single peak emission, which gradually shifts to longer wavelengths, from green to yellow to orange to red, with increasing reflux time and particle size. At longer reflux times, deconvolution of the emission peak into Gaussian components was done to qualitatively investigate the contribution of emission from different sized particles, as can be seen in the inset of Fig.4; comparison of the component peaks at different times suggests that as reflux time increases, emission intensity contribution from larger particle sizes increases. Zetapotential analysis was conducted to obtain the surface charge of the synthesised thiol-capped CdTe QDs to study the effect the different functional groups on the surface of the QD; DLS analysis was conducted to obtain the hydrodynamic diameter of the synthesised thiol-capped CdTe QDs.

1. I. L. Medintz, H. T. Uyeda, E. R. Goldman, H. Mattoussi, *Nature Materials*, **4(6)**, (2005), 435.
2. X. Gao, Y. Cui, R. M. Levenson, L. W. Chung, S. Nie, *Nature Biotechnology*, **22(8)**, (2004), 969.
3. C. Y. Zhang, H. C. Yeh, M. T. Kuroki, T. H. Wang, *Nature Materials*, **4(11)**, (2005), 826.
4. D. V. Talapin, S. Haubold, A. L. Rogach, A. Kornowski, M. Haase, H. Weller, *The Journal of Physical Chemistry B*, **105(12)**, (2001), 2260.
5. N. Gaponik, A. L. Rogach, *Physical Chemistry Chemical Physics*, **12(31)**, (2010), 8685.
6. L. Qi, X. Gao, *Expert Opinion on Drug Delivery*, **5(3)**, (2008), 263.



SL6

IN-SITU LOADING ON DEFECT CONTAINING MATERIAL OBSERVED UNDER HIGH-RESOLUTION TOMOGRAPH

Ahmed Ubaid

Institute of Physics, Czech Academy of Sciences, Na Slovance 1999/2, 180 00 Praha 8

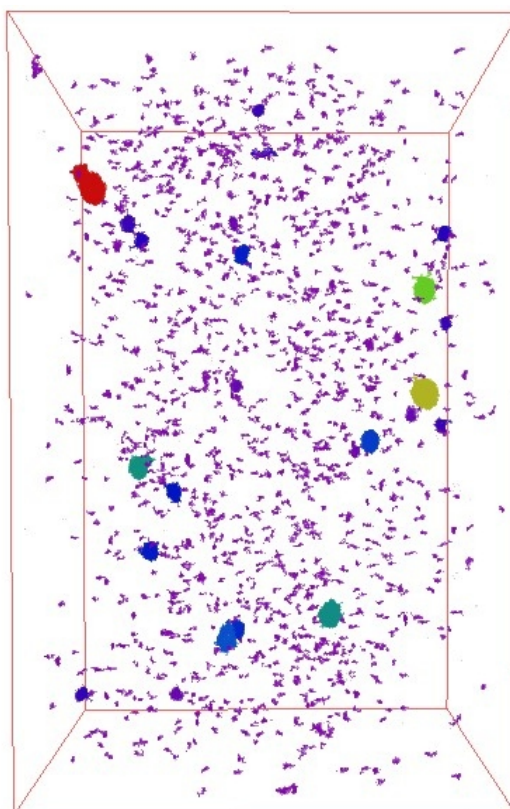
NiTi possess unique shape memory and pseudoelastic characteristics. In this research, a dog-bone shaped sample of NiTi is being analysed under X-ray Computed Tomography. Deformation characteristics of NiTi have been studied due to their increased demand in the miniaturized applications. The in-situ tensile testing was performed at -20C with different load i.e., 10N, 150N, 220N and 300N using Deben chamber of Xradia Versa 610, Zeiss. The sample had 4.2 mm gauge length, 1 mm width and 1 mm height. The reconstructed images and large number of pores/inclusions were being analysed using DragonFly software. Images obtained under different loading were

compared, dimensional changes in the pores/inclusions were determined as well as changes in the distances amongst different pores were calculated. The sample showed 1 % deformation at 150N, 3.80 % at 220N and 5.4 % deformation at 300N.

1. Otani, J., & Obara, Y. (Eds.). (2004). Xray CT for Geomaterials: Soils, Concrete, Rocks International Workshop on Xray CT for Geomaterials, Kumamoto, Japan. CRC Press.
2. Carmignato, S., Dewulf, W., & Leach, R. (Eds.). (2018). Industrial X-ray computed tomography. Cham: Springer International Publishing.

PD: 2.70 mm

W: 454 C: 27,761



-5

Figure 1. Different size pores shown with different colours at 220 N and -2 0°C.